Inorganic Chemistry

Article

pubs.acs.org/IC

Solid-State Emissive B,S-Bridged *p*-Terphenyls: Synthesis, Properties, and Utility as Bifunctional Fluorescent Sensor for Hg^{2+} and F^- Ions

Dong-Mei Chen,[†] Sheng Wang,[†] Hong-Xiang Li,[‡] Xiao-Zhang Zhu,[§] and Cui-Hua Zhao*[,†]

[†]School of Chemistry and Chemical Engineering, Key Laboratory of Special Functional Aggregated Materials, Ministry of Education, Shandong University, Jinan 250100, People's Republic of China

[‡]Shanghai Institute of Organic Chemistry, Chinese Academy of Sciences, Shanghai 200032, People's Republic of China

[§]Beijing National Laboratory for Molecular Sciences, Key Laboratory of Organic Solids, Institute of Chemistry, Chinese Academy of Sciences, Beijing 100190, People's Republic of China

Supporting Information

ABSTRACT: The efficient synthesis has been disclosed to achieve a new class of ladder-type molecules, B,S-bridged *p*-terphenyls (**BS-TPs**). Their properties were fully characterized by UV−vis and fluorescence spectroscopy in both solution and solid state, time-resolved fluorescence spectroscopy, DFT theoretical calculations, and cyclic voltammetry. A detailed comparison between ***anti*-BS-TP** and its analogue B,N-bridged *p*-terphenyl (**BN-TP**) was made to elucidate the effect of displacement of bridging N with S atom on the properties. The introduction of S rather than N atom as bridging atom leads to increased fluorescence efficiency in both solution and solid state as well as enhanced reduction stability. And thus this new class of ladder-type molecules are highly emissive in both solution and solid state and display reversible reduction wave in cyclic voltammograms, denoting their promising potentials as electron-transporting solid-state emitters. In addition, this new class of molecules are capable of detecting F^- and Hg^{2+} with different fluorescence responses, owing to the high Lewis acidity of the B center to coordinate with F^- anions and the great mercury-philicity of the S center to complex with Hg^{2+} cations.

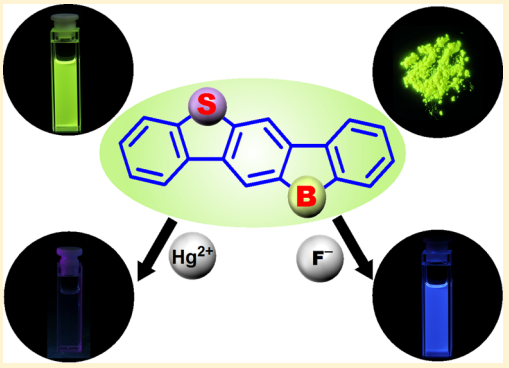

INTRODUCTION

Over the past decade, the ladder-type polycyclic aromatic hydrocarbons have emerged as a promising class of materials because of their rigid planar structure, which would lead to efficient electron delocalization and strong intermolecular $\pi-\pi$ interactions and therefore highly desirable electronic and photophysical properties, such as intense fluorescence and high carrier mobility. The extensive investigations on this class of compounds have demonstrated their potential applications in various optoelectronic fields, such as organic field-effect transistors (OFETs), organic light emitting devices (OLEDs), and organic photovoltaics (OPVs).[1] As a representative example, ladder-type oligo(*p*-phenylene)s (LOPPs) with carbon as bridging atoms have well been utilized as efficient emitters in OLEDs, owing to their high fluorescence efficiency.[2] To modulate the frontier molecular orbitals and thus optoelectronic properties, embedding heteroatoms such as N,[3] O,[4] and S[5] within polycyclic aromatic molecules have proved to be an efficient strategy due to their special orbital interactions with the attached π-conjugated framework. For instance, the displacement of the bridging carbon with a N or S atom in the LOPPs can endow the corresponding systems with great capacity to be used as p-type materials in OFETs as the result of the electron-donating ability of N and S atoms.

In addition to the traditional hetero elements, the main group elements, such as B,[6] Si,[7] and P,[8] have recently attracted increasing consideration because they can provide more opportunities in property tuning via heteroatom coordination number change, heteroatom oxidation, or functionalization in addition to orbital interactions. Among them, the B element is particularly interesting for the creation of new organic optoelectronic materials. The most important feature of a trivalent boron center in a π-conjugated framework is its vacant p-orbital, allowing effective electron delocalization throughout the whole system.[9] The research on the B-bridged biphenyl (dibenzoborole) has demonstrated that it can act as an efficient electron-accepting unit. Despite a number of B-bridged ladder-type π-systems,[10] those with integration of both boron and electron-donating atoms are very limited due to the difficulty in the synthesis.[11] To this end, we have recently established an efficient synthetic route to a new class of ladder-type π-conjugated molecules, B,N-bridged *p*-terphenyls (**BN-TPs**), in which both the electron-accepting B atom and electron-donating N atom are introduced as bridging atoms.[12] The incorporation of B, N atoms makes this system exhibit both oxidation and reduction potentials, which are important for bipolar-transporting properties. In addition, more recent observation revealed that this class of compounds showed no fluorescence quenching in the solid state (Φ_F = 0.21 in

Received: August 28, 2014
Published: November 4, 2014

   dx.doi.org/10.1021/ic502088k | *Inorg. Chem.* 2014, 53, 12532−12539

cyclohexane; 0.22 in spin-coated film for ***anti*-BN-TP**). The fascinating properties and facile synthetic route of **BN-TPs** encouraged us to prepare another class of boron-containing ladder-type molecules, B,S-bridged *p*-terphenyls (**BS-TPs**, Figure 1). It was fascinating to find that the displacement of

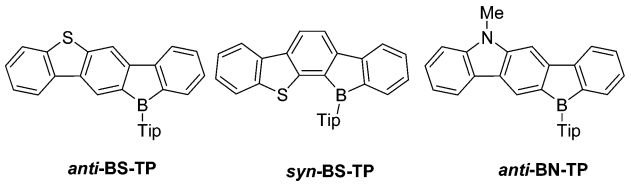

Figure 1. Structures of **BS-TPs** and ***anti*-BN-TP**.

bridging N with S atom led to a remarkable increase of fluorescence efficiency in both solution and solid state and enhanced reversibility of reduction in the cyclic voltammogram. To elucidate the effect of displacement of bridging N with S atom on properties, a detailed comparison was made between ***anti*-BS-TP** and its analogue ***anti*-BN-TP**, in terms of absorption and emission in solution and solid state, time-resolved fluorescence, theoretical calculations, as well as electrochemical properties. In addition, we also explored the application of this new type of molecules as a bifunctional fluorescent sensor to detect Hg^{2+} and F^- simultaneously, utilizing the high Lewis acidity of the B center to coordinate with F^- anions and the great mercury-philicity of the S center to complex with Hg^{2+} cations.

RESULTS AND DISCUSSION

Synthesis. The synthesis of **BS-TPs** was accomplished in six steps starting from a triazene derivative **1**,[13] as illustrated in Scheme 1. Thus, the first Pd(0)-catalyzed Suzuki–Miyaura

Scheme 1. Synthesis of BS-TPs

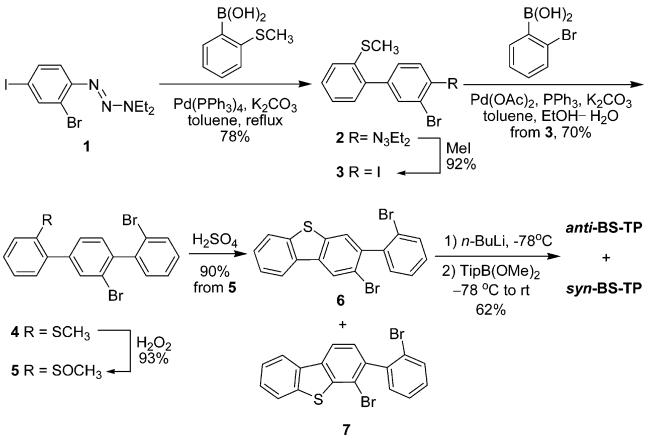

coupling reaction of **1** with 2-thioanisoleboronic acid and subsequent iodination of the triazeno group afforded compound **3**, the Suzuki–Miyaura coupling of which with 2-bromophenylboronic acid followed by oxidation with H_2O_2 produced the main synthetic intermediate, sulfinyl derivative **5**. The ring-closing condensation of **5** under concentrated sulfuric acid proceeded smoothly to give a mixture of dibenzothiophene derivatives **6** and **7**.[14] It was noted that the R_f values of compounds **6** and **7** on TLC are completely the same. As a result, they were used directly as a mixture in the next step reaction. In the ^{1}H NMR spectrum of the mixture of compounds **6** and **7** (Figure S1), the singlet at 8.44 ppm is assignable to one proton of compound **6** and the multiplet at 7.69–7.22 ppm corresponds to one proton of **6** and one proton of **7**. Based on the integration of these two signals, the ratio between **6** and **7** is deduced to be about 4.35:1. Therefore, the ring-closing of **5** takes place dominantly at the *p*-position of bromide, which is probably ascribed to the influence of the steric effect of the bromo substituent. Finally, the **BS-TPs** were obtained via the dilithiation of the mixture of **6** and **7** followed by electronic quenching with $TipB(OMe)_2$. Fortunately, the separation of ***anti*-BS-TP** from ***syn*-BS-TP** was achieved via flash chromatography due to their different R_f values. Although the chemical stability of ***syn*-BS-TP** is greatly improved compared with the corresponding ***syn*-BN-TP** analogue due to the absence of a substituent on the S atom and thus less steric hindrance, the ***syn*-BS-TP** still shows lower chemical stability than its regioisomer ***anti*-BS-TP**. The ***anti*-BS-TP** is stable in various solvents while ***syn*-BS-TP** decomposes gradually in polar organic solvents such as THF and MeCN, as monitored by TLC. The lower chemical stability of ***syn*-BS-TP** might also be due to the influence of the steric congestion, which would facilitate the ring-opening of borole.[12]

Photophysical Properties in Solutions. The photophysical properties were first measured in cyclohexane solutions. The UV/vis absorption and emission spectra are shown in Figure 2, the data for which are listed in Table 1. With

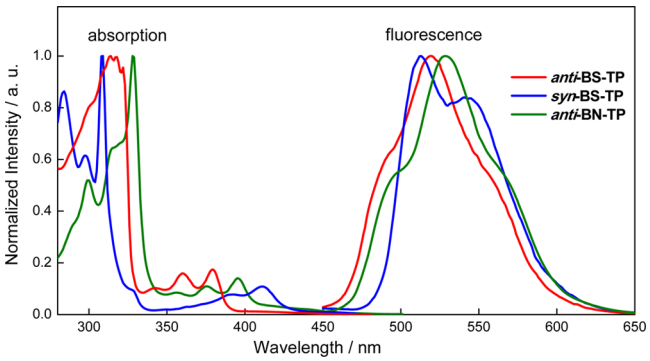

Figure 2. UV/vis absorption and emission spectra (λ_{ex} = 360 nm) of **BS-TPs** and ***anti*-BN-TP**.

regard to the photophysical properties, we are here particularly curious about the effect of displacement of the bridging N atom with an S atom. To elucidate this point, we made a comprehensive comparison between ***anti*-BS-TP** and its B,N-bridged analogue, ***anti*-BN-TP**. The B,S bridged *p*-terphenyl ***anti*-BS-TP** displays a moderately intense absorption at 380 nm and bright yellowish green fluorescence at 519 nm. Compared with its analogue ***anti*-BN-TP**, the displacement of the N atom with an S atom induces only slight hypochromism in both absorption and fluorescence spectra ($\Delta\lambda$ = 15 nm, 999 cm^{-1} for absorption; 10 nm, 364 cm^{-1} for emission). A notable common feature for these two analogues is that their Stokes shifts are rather large for such a rigid planar structure, which generally leads to a small Stokes shift due to the restricted structural relaxation in the excited state. Most notably, the fluorescence of ***anti*-BS-TP** is rather brighter than ***anti*-BN-TP** with quantum yield two times higher (Φ_F = 0.21 for ***anti*-BN-TP**; 0.55 for ***anti*-BS-TP** in cyclohexane). The sulfur-containing ladder-type molecules have been well utilized as carrier-transporting

dx.doi.org/10.1021/ic502088k | *Inorg. Chem.* 2014, 53, 12532–12539

Table 1. Photophysical Properties of BS-TPs and *anti*-BN-TP in Cyclohexane

	absorption	fluorescence		excited-state dynamics		
	λ_{abs} (nm)[a] (log ε)	λ_{em} (nm)	Φ_F[b]	τ (ns)	k_r (s^{-1})	k_{nr} (s^{-1})
anti-**BS-TP**	380 (3.75)	519	0.55	78.7	7.0×10^6	5.7×10^6
syn-**BS-TP**	411 (3.81)	513	0.42	75.2	7.3×10^6	10.2×10^6
anti-**BN-TP**	395 (3.92)	529	0.21	82.5	2.5×10^6	9.6×10^6

[a]Only the longest maxima are shown. [b]Calculated using fluorescein as standard.

materials,[15,5b] but seldom as emitting materials due to their low fluorescence efficiency as the result of the heavy atom effect of sulfur,[16] which would generally facilitate the nonradiative decay through intersystem crossing. To have a deep insight into the effect of displacement of the bridging N with S atom on emission, we also determined the fluorescence lifetime and calculated the radiative (k_r) and nonradiative (k_{nr}) decay rate constants from the singlet excited state, based on the equations $\Phi_F = k_r \times \tau_s$ and $k_r + k_{nr} = \tau^{-1}$ (Table 1). The time-resolved fluorescence study showed that the fluorescence lifetimes of ***anti*-BS-TP** and ***anti*-BN-TP** are very close (τ = 78.7 ns for ***anti*-BS-TP**; 82.5 ns for ***anti*-BN-TP**). And the increase in the fluorescence efficiency from ***anti*-BN-TP** to ***anti*-BS-TP** is owing to the acceleration of radiative decay and deceleration of the nonradiative process, which is different from the normal S-containing π-system. Herein our results provide an example of an emissive S-bridged ladder-type π-conjugated system.

As for the effect of the relative position of the bridging B and S atoms on the photophysical properties, similar changes were observed in the absorption and emission from the *anti*-type to the *syn*-type isomer as in the B,N-bridged *p*-terphenyl system.[12] Namely, from ***anti*-BS-TP** to ***syn*-BS-TP**, the absorption shifts to longer wavelength by a large extent ($\Delta\lambda$ = 31 nm, 1984 cm^{-1} for the longest absorption band) while the emission exhibits no great shift in position, which is associated with a slight decrease in the fluorescence efficiency. The decrease of fluorescence efficiency from ***anti*-BS-TP** to ***syn*-BS-TP** is mainly ascribed to the acceleration of the nonradiative decay process based on the time-resolved fluorescence study (Table 1). Another notable characteristic for this B,S-bridged *p*-terphenyl system is that neither absorption nor fluorescence spectra show obvious solvatochromism (Figure S2), similar to their B,N-bridged analogues.[12] The trivial solvatochromism on both absorption and emission indicates the small polarity change from the ground state to the excited state.

Electrochemical Properties. The electrochemical properties of the B,S-bridged *p*-terphenyls **BS-TPs** and the analogue ***anti*-BN-TP** were studied by means of cyclic voltammetry. Their cyclic voltammograms (CV) are shown in Figure 3. All these compounds display both oxidation and reduction peaks in the CV diagrams, possibly owing to the presence of both the electron-donating S or N and the electron-withdrawing B atoms. It is interesting to note that the reduction of **BS-TPs** is totally reversible while ***anti*-BN-TP** only shows an irreversible reduction wave, demonstrating that the introduction of S instead of N as bridging atom can stabilize the formed anionic radicals. Based on the redox potentials, the HOMO and LUMO energy levels were estimated using the onset of the corresponding redox waves and are referenced to ferrocence, which has a HOMO of −4.8 eV. The corresponding experimental HOMO/LUMO energy levels are shown in Figure 4. From ***anti*-BN-TP** to ***anti*-BS-TP**, the HOMO energy level is lowered by 0.57 eV while the LUMO energy level remains almost unchanged, which leads to a larger energy gap.

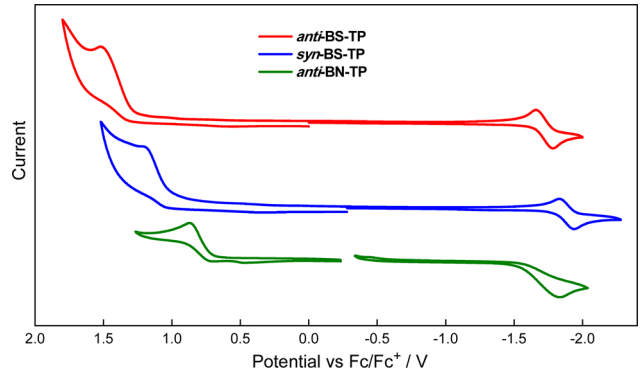

Figure 3. Cyclic voltammograms of **BS-TPs** and ***anti*-BN-TP** (1 mM), measured with TBAP (tetrabutylammoniumperchlorate, 0.1 M) as the supporting electrolyte at a scan rate of 100 mV/s.

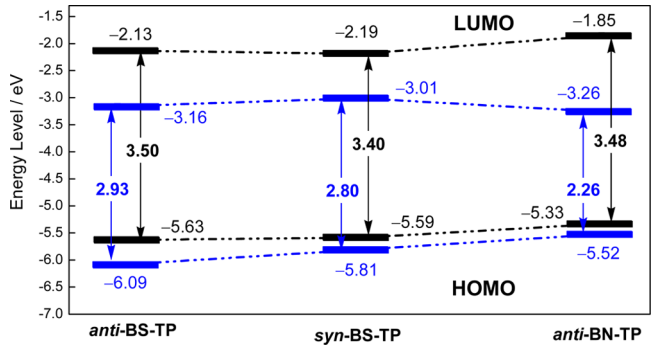

Figure 4. Experimental (blue lines) and calculated (black lines) energy levels of **BS-TPs** and ***anti*-BN-TP**.

The decreased HOMO energy level might be ascribed to the weaker electron-donating ability of the S atom compared with the N atom. With regard to the effect of the relative position of the bridging B and S atoms, both the HOMO and LUMO shift to higher energy from ***anti*-BS-TP** to its regioisomers ***syn*-BS-TP**. In addition, the energy gap becomes smaller as the result of greater elevation of the HOMO (0.28 eV) relative to the LUMO (0.15 eV).

Theoretical Calculations. To elucidate the influence of the displacement of the bridging N with an S atom and the effect of the relative positions of B and S on the electronic structures and thus photophysical properties, we conducted theoretical calculations of the newly prepared **BS-TPs** and the analogue ***anti*-BN-TP**. The optimizations of the molecular geometry and total energy calculations were carried out using density-functional theory (DFT) calculations at the B3LYP/6-31G(d) level of theory. The pictorial drawings of their molecular orbitals are shown in Figure 5, and the calculated data are summarized in Table 2. The electronic distributions are very similar for **BS-TPs** and ***anti*-BN-TP**. Thus, the HOMOs are delocalized over the entire *p*-terphenyl framework with some

dx.doi.org/10.1021/ic502088k | *Inorg. Chem.* 2014, 53, 12532−12539

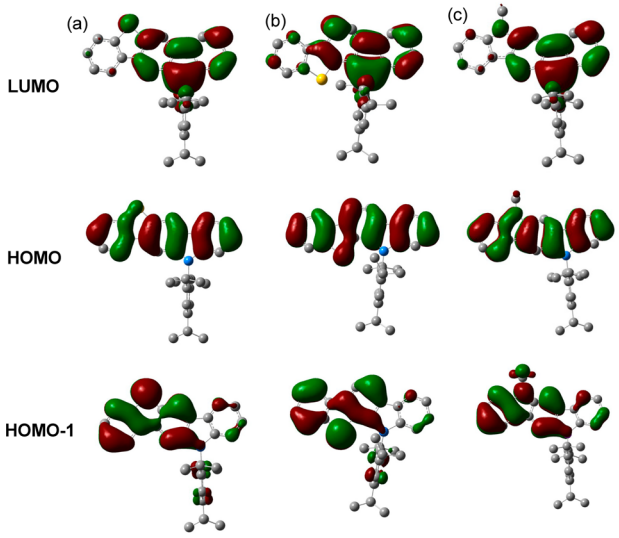

Figure 5. Associated molecular orbitals that are likely responsible for the low-energy absorption bands of (a) ***anti*-BS-TP**; (b) ***syn*-BS-TP**; and (c) ***anti*-BN-TP**.

contribution from the electron-donating hetero S and N atoms. And the HOMO−1 orbitals are mainly localized on dibenzothiophene or carbazolyl moiety. In contrast, the LUMOs are dominantly located on the dibenzoborole moiety with remarkable contribution from the vacant p orbital on the B atom. Although the change of the bridging atom from N to S has a trivial influence on the electronic distribution of the frontier orbitals, obvious differences are still observed in the frontier orbital energy levels. From ***anti*-BN-TP** to ***anti*-BS-TP**, the HOMO energy level is lowered by 0.30 eV, with almost the same extent as LUMO (0.28 eV). It is notable that the HOMO−1 decreases with a larger degree (0.37 eV), which is reasonable considering the greater electron distribution on the bridging S or N atom in the HOMO−1 than that in the HOMO and LUMO orbitals. In view of the effect of the relative position of the bridging B and S atoms, the occupied HOMO and HOMO−1 orbitals are elevated by 0.04 and 0.11 eV, respectively, whereas the LUMO decreases by 0.06 eV from ***anti*-BS-TP** to its regioisomers ***syn*-BS-TP**. As a result, the energy gap of ***syn*-BS-TP** becomes narrower relative to ***anti*-BS-TP**. A noteworthy common trend in the change of orbital levels is that both the displacement of the bridging N with an S atom and the change of the relative positions of the bridging S and B atoms exhibit greater influence on the HOMO−1 energy level than on the HOMO and LUMO energy levels.

To shed light on the nature of their absorptions, we also performed time-dependent density-functional theory (TD-DFT) calculations at the B3LYP/6-31G(d) level of theory. The results are also included in Table 2. It is noteworthy that the longest absorptions are in fact ascribed to the electronic transition from HOMO−1 to the LUMO, rather than the lowest excited state transition (S_1) from HOMO to LUMO. The oscillator strengths of the S_1 states are very low for all these ladder-type molecules, which would make the lowest transition band too weak to be distinguished and thus partially account for their large Stokes shift. Based on the assignment of absorptions, it is easily understandable that the absorption spectra display more obvious changes than the fluorescence spectra due to the larger difference of the HOMO−1 energy level than the HOMO and LUMO from ***anti*-BN-TP** to ***anti*-BS-TP** and from ***anti*-BS-TP** to ***syn*-BS-TP**. In addition, the trivial solvatochromism on emission is also reasonable considering that the fluorescence occurs from the lowest excited state, in which the charge separation might be not very significant because the location of the positive center is probably very close to the center of the molecular structure and thus the negative boron center, as the result of the highly efficient electron delocalization in the ground state. Due to the limitation of the ground-state DFT calculations, there exist some discrepancies of HOMO/LUMO energy levels between calculated and experimental values, and the general trend of the calculated energy gaps almost agrees with the experimentally observed trend. In addition, these calculated results clearly indicate that the displacement of the bridging N with an S atom and the change of the relative positions of bridging S and B atoms have a great influence on the frontier occupied molecular orbital energies, which is also consistent with the experimental results.

Photophysical Properties in the Solid-State. The increased fluorescence efficiency from ***anti*-BN-TP** to ***anti*-BS-TP** in solution and no significant fluorescence quenching of ***anti*-BN-TP** in the solid state encouraged us to measure the photophysical properties of **BS-TPs** in the solid state. Thin films of **BS-TPs** were spin-coated from their solutions in dichloromethane with approximately 3 mg mL^{-1} concentration

Table 2. Calculated Kohn−Sham Molecular Orbital Energy Levels and the Calculated Vertical Excited States for BS-TPs and *anti*-BN-TP

				excited state								
				S_1			S_2			S_3		
	HOMO−1 (eV)	HOMO (eV)	LUMO (eV)	transition	energy (nm)	oscillator strength	transition	energy (nm)	oscillator strength	transition	energy (nm)	oscillator strength
***anti*-BS-TP**	−5.94	−5.63	−2.13	H→L (97%)	449	0.0029	H−2→L (94%)	402	0.0036	H−1→L (68%)	373	0.0776
										H−3→L (18%)		
***syn*-BS-TP**	−5.83	−5.59	−2.19	H→L (98%)	463	0.0101	H−2→L (86%)	415	0.0079	H−1→L (83%)	405	0.068
							H−1→L (13%)			H−2→L (12%)		
***anti*-BN-TP**	−5.57	−5.33	−1.85	H→L (96%)	452	0.003	H−2→L (66%)	386	0.0475	H−1→L (57%)	383	0.0475
							H−1→L (28%)			H−2→L (32%)		

dx.doi.org/10.1021/ic502088k | *Inorg. Chem.* 2014, 53, 12532−12539

on the quartz plates, and their absorption and emission were directly measured (Figure 6). The absolute quantum yields of spin-coated films were determined by a calibrated integrating sphere system, and the corresponding data are summarized in Table 3.

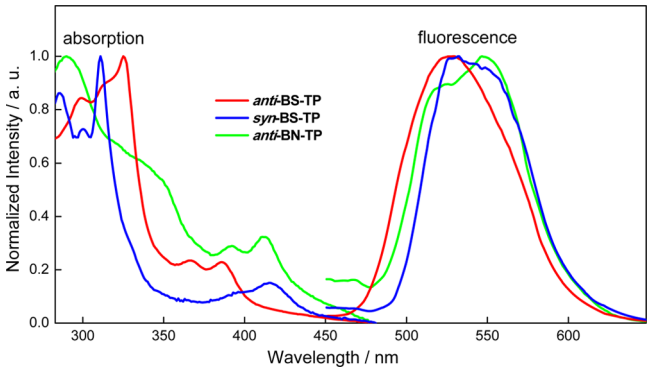

Figure 6. UV/vis absorption and emission spectra (λ_{ex} = 360 nm) of **BS-TPs** and ***anti*-BN-TP** in spin-coated films.

Table 3. Photophysical Properties of BS-TPs and *anti*-BN-TP in Spin-Coated Films

	λ_{abs} (nm)[a]	λ_{em} (nm)	Φ_F[b]
***anti*-BS-TP**	386	529	0.44
***syn*-BS-TP**	416	531	0.33
***anti*-BN-TP**	412	547	0.22

[a]Only the longest maxima are shown. [b]Absolute quantum yield determined by the calibrated integrating sphere system.

These two **BS-TPs** only display a slight decrease of fluorescence efficiency from solution to the spin-coated film. And the fluorescence quantum yields of both **BS-TPs** are higher than that of the B,N-bridged analogue ***anti*-BN-TP**. Especially, ***anti*-BS-TP** displays very bright yellowish green fluorescence in the solid-state with quantum yield two times higher relative to ***anti*-BN-TP**. Most of the ladder-type molecule displays severe fluorescence quenching due to the planar structure, which would lead to the strong intermolecular $\pi-\pi$ interactions. In these ladder-type molecules, the bulky Tip group on the B atom is very effective to prevent intermolecular interactions, as evidenced by the high similarity of absorption and emission spectra in solution and solid state (Figure S3). Another factor that might be responsible for the retained fluorescence in the solid state is the large Stokes shift, which would prevent the nonradiative decay of long distance energy transfer. In view of the desired properties of **BS-TPs**, especially ***anti*-BS-TP**, including reversibility of the reduction process and high fluorescence efficiency in solution and solid state, they might be applied as electron-transporting solid-state emitters.

Utility as Bifunctional Fluorescent Sensor of F^- and Hg^{2+}. The detection of fluoride and mercury is of great interest because they are highly relevant to human health and environmental issues. Triarylboranes have been well utilized as effective fluoride sensors due to the high Lewis acidity of the boron center to coordinate with fluoride anions. The coordination of the boron atom with basic fluoride anions would disrupt the $p_\pi-\pi^*$ conjugation between the boron center and the attached π-conjugated framework and thus lead to remarkable changes in UV/vis absorption, fluorescence, and two-photon excited fluorescence.[17−20] Despite the extensive utilization of triarylboranes as fluoride sensor, the examples that can be used as bifunctional sensor to detect fluoride and other ions simultaneously are very limited. In **BS-TPs**, in addition to the electron-accepting boron center, there exists a mercury-philic sulfur center. Many S-containing sensors have recently been designed to detect Hg^{2+} based on the highly thiophilic nature of Hg^{2+}.[21] Considering the high Lewis acidity of B to bind with F^- and the intense mercury-philicity of S to complex with Hg^{2+}, we herein were interested in whether F^- and Hg^{2+} would react with B and S atoms in **BS-TPs** and consequently result in the great changes in absorption and emission spectra. And thus we next explored the sensing ability of **BS-TPs** to detect F^- and Hg^{2+} simultaneously using ***anti*-BS-TP** as a representative compound.

The titration of ***anti*-BS-TP** with F^- was carried out in THF by using nBu$_4$NF (TBAF) as fluoride sources. The spectra changes of ***anti*-BS-TP** (20 μM) upon addition of TBAF are shown in Figure 7. In THF solution, ***anti*-BS-TP** displays the

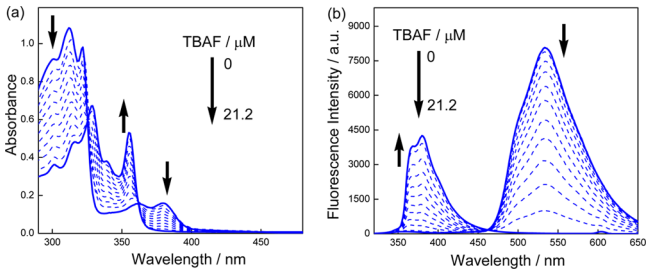

Figure 7. (a) Absorption and (b) fluorescence spectra (λ_{ex} = 325 nm) changes of ***anti*-BS-TP** in THF solution (20 μM) upon addition of TBAF.

longest absorption at 380 nm and intense yellowish green fluorescence at 535 nm. Upon addition of TBAF, the absorption at 380 nm decreased gradually with the appearance of a blue-shifted band at 355 nm. At the same time, the emission at 535 nm was also blue-shifted to 380 nm. The changes in absorption and emission of ***anti*-BS-TP** were reasonable considering the large contribution of the B atom to the LUMO via $p_\pi-\pi^*$ conjugation, which would be interrupted upon binding of fluoride ions to the boron center. And the changes became saturated when the concentration of TBAF amounted to 21.2 μM. The binding constant was determined to be 4.45×10^4 M^{-1} (Figure S4), which is a little bit lower than those of other tricoordinate organoboron compounds.[17−20] It was noted that the fluorescence still remained very intense irrespective of the binding mode and the ratios of emission intensities at 380 and 535 nm (I_{380}/I_{535}) exhibit a dramatic change from 0.007:1 to 300.2:1, demonstrating its ratiometric fluorescence sensing for fluoride. Moreover, an obvious color change of fluorescence was also observed from yellowish green to sky blue, thus enabling colorimetric sensing of fluoride anions by naked eyes.

To examine the sensing ability of ***anti*-BS-TP** toward Hg^{2+} cations, the titration experiments were conducted in THF solution using mercury(II) perchlorate as Hg^{2+} resource. The spectra changes of ***anti*-BS-TP** (20 μM) upon addition of Hg^{2+} are shown in Figure 8. The incremental addition of Hg^{2+} cations resulted in the gradual quenching of the absorption at 380 nm and the intense fluorescence at 535 nm. The quenching of fluorescence was associated with the remarkable fluorescence color change from yellowish green to colorless. The sensing

dx.doi.org/10.1021/ic502088k | Inorg. Chem. 2014, 53, 12532−12539

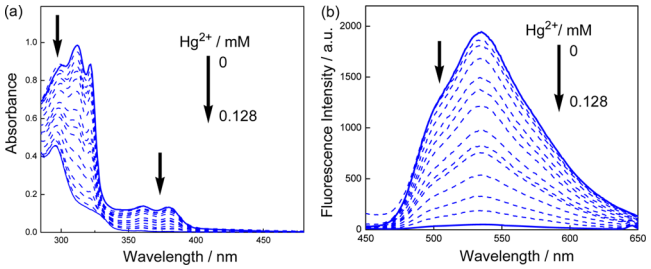

Figure 8. (a) Absorption and (b) fluorescence spectra (λ_{ex} = 360 nm) changes of *anti*-BS-TP in THF solution (20 μM) upon addition of Hg^{2+}.

ability of ***anti*-BS-TP** toward Hg^{2+} is presumably due to complexation of the bridging S atom with Hg^{2+}.[21] The stoichiometry analysis through the Job plot suggests the formation of a 1:1 complex (Figure S5). And the binding constant calculated from fluorescence titration data is 3.57 × 10^3 M^{-1} (Figure S6), which is also lower than those of other S-containing sensors.[21] The decreased binding ability of ***anti*-BS-TP** to F^- and Hg^{2+} might result from the more significant conjugation of this rigid π-conjugated framework, which would lead to more delocalization of lone pair electrons on the sulfur atom and decreased Lewis acidity of the tricoordinate boron atom. In addition, only the addition of Hg^{2+} resulted in the prominent absorption and emission changes among various examined competitive cations, such as Na^+, K^+, Li^+, Cd^{2+}, Mg^{2+}, Mn^{2+}, Zn^{2+}, Ni^{2+}, and even Ag^+, suggesting the high selectivity of ***anti*-BS-TP** in sensing of Hg^{2+} over other cations (Figure 9).

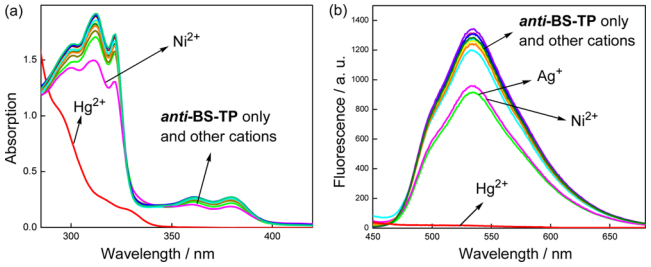

Figure 9. (a) Absorption and (b) fluorescence spectra (λ_{ex} = 360 nm) of *anti*-BS-TP in THF solution (20 μM) upon addition of various metal ions (30 equiv).

It is most noteworthy that the changes in fluorescence of ***anti*-BS-TP** are quite different upon addition of F^- and Hg^{2+}. The fluorescence remains very intense irrespective of the binding of B with F^- while the fluorescence is almost completely quenched upon complexation of S with Hg^{2+}. The current results of titration experiments clearly suggest the excellent ability of ***anti*-BS-TP** to be used as bifunctional fluorescent sensor to detect F^- and Hg^{2+} simultaneously.

CONCLUSION

In summary, we have established an efficient synthetic route to a new class of ladder-type π-conjugated molecules, B,S-bridged *p*-terphenyls (**BS-TPs**). Compared with the previously reported analogue, B,N-bridged *p*-terphenyl (**BN-TP**), this class of compounds display increased fluorescence efficiency in solution and solid state as well as enhanced reduction stability in cyclic voltammograms. And thus this new class of ladder-type molecules are highly emissive in both solution and solid state and display reversible reduction waves in cyclic voltammograms, denoting their promising potentials as electron-transporting solid-state emitters. A detailed comparison between ***anti*-BS-TP** and its analogue, ***anti*-BN-TP**, was made to elucidate the effect of the displacement of bridging N with S atom on the properties, in terms of UV−vis absorption and fluorescence in solution and solid state, time-resolved fluorescence, DFT theoretical calculations, and electrochemical properties. In addition, this new class of molecules are capable of detection of F^- and Hg^{2+} at the same time, owing to the high Lewis acidity of the B center to coordinate with F^- anions and the great mercury-philicity of the S center to complex with Hg^{2+} cations. We herein have not only disclosed a new class of boron-containing ladder-type molecules with promising properties but also provided a useful basis for the further rational design of functional boron-containing ladder-type molecules and bifunctional triarylboron-based sensors via the elucidation of structure−property relationships.

EXPERIMENTAL SECTION

Caution! *n-BuLi was used during the course of the experimental work. It is a very reactive reagent. It may react violently with water to give off flammable gases and corrosive dusts. Experiments using n-BuLi were carried out with the protection of N_2 to keep away from water, air, and oxidizing materials. In addition, the storage container should be protected from leaks and physical damage.*

General. Melting points (mp) were measured on a Tektronix XT-4 instrument. ^1H and ^{13}C NMR spectra were recorded with a Bruker 300 spectrometer or a Bruker 400 spectrometer in $CDCl_3$. High-resolution mass spectra (HRMS) were recorded on an Agilent Q-TOF 6510 LC/MS mass spectrometer using the electrospray ionization (ESI) technique for compounds **2**−**5** and an IonSpec 4.7 T FTMS mass spectrometer using the matrix-assisted laser desorption ionization (MALDI) technique for other compounds. All reactions were carried out under nitrogen atmosphere. Compound **1** was prepared according to the literature.[13]

Photophysical Measurements. UV−vis absorption and fluorescence spectra measurement (the titration experiments for exception) were performed with a Hitachi UV-4100 spectrometer and a Hitachi F-4500 spectrometer, while the absorption and fluorescence spectra of titration experiments were collected with a TU-1901 spectrometer (Beijing Purkinje General Instrument) and a Hitachi F-7000 spectrometer. The fluorescence lifetimes were measured with an Edinburgh Fluorescence Measurement System FLS920 equipped with an ultrafast nanosecond flash lamp nF920 (excitation wavelength 360 nm) using a time correlated single photon counting (TCSPC) method. Spin-coating was carried out using JYL YJ-150 at room temperature. The spin-coated films were prepared by spinning the dichloromethane solutions (3 mg mL^{-1}) onto quartz plates at 1000 rpm for 30 s. The quantum yields of spin-coated films were measured using a calibrated integrating sphere system (FLS920, Edinburgh Instruments).

Computational Methods. The geometries of **BS-TPs** in the ground state were optimized using density functional theory (DFT) at the B3LYP/6-31G(d) level of theory by Gaussian 09 program.[22] All geometry optimizations were followed by a frequency calculation to ensure that the optimized geometry was at a minimum. The time-dependent density functional theory (TD-DFT) calculations were conducted at the B3LYP/6-31G(d) level of theory.

Electrochemical Measurements. Cyclic voltammetry (CV) was performed using a BSA 100W instrument with a scan rate of 100 mV/s. A three-electrode configuration was used for the measurements: a platinum electrode as the working electrode, a platinum wire as the counter electrode, and an Ag/Ag^+ electrode as the reference electrode. A 0.1 M solution of TBAP in the THF was used as the supporting electrolyte. The ferrocene/ferrocenium (Fc/Fc^+) couple was used as the internal standard.

3′-Bromo-4′-(3,3-diethyltriazeno)-2-methylthio[1,1′]-biphenyl (2). To a solution of **1** (4.57 g, 12.0 mmol), 2-

dx.doi.org/10.1021/ic502088k | *Inorg. Chem.* 2014, 53, 12532−12539

thioanisoleboronic acid (2.35 g, 14.4 mmol) and $Pd(PPh_3)_4$ (139 mg, 0.12 mmol) in degassed toluene (120 mL) was added a degassed solution of K_2CO_3 (24 mL, 2.0 M) under a steam of nitrogen. The reaction mixture was refluxed overnight. The mixture was cooled to room temperature and then extracted with CH_2Cl_2. The combined organic layer was dried over anhydrous Na_2SO_4, filtered, and concentrated under reduced pressure. The resulting mixture was subjected to a silica gel column chromatography (5/1 petroleum ether/CH_2Cl_2, R_f = 0.29) to afford 3.54 g (9.39 mmol) of **2** in 78% yield as yellow solids: mp 67−68 °C; ^{1}H NMR ($CDCl_3$, 300 MHz): δ 1.22 (t, J = 7.2 Hz, 6H), 2.29 (s, 3H), 3.69 (q, J = 7.2 Hz, 4H), 7.07−7.25 (m, 5H), 7.36 (d, J = 8.1 Hz, 1H), 7.57 (s, 1H); ^{13}C NMR ($CDCl_3$, 75 MHz): δ 11.1, 14.5, 16.1, 42.1, 49.2, 117.8, 119.5, 124.8, 125.5, 128.0, 128.9, 130.0, 133.7, 137.3, 138.3, 139.6, 147.7; HRMS (ESI): 378.0641 ([M + H]$^+$); Calcd for $C_{17}H_{21}BrN_3S$: 378.0640.

3′-Bromo-4′-iodo-2-methylthio[1,1′]biphenyl (3). A solution of triazene derivative **2** (0.94 g, 2.5 mmol) in iodomethane (4.7 mL, 75.0 mmol) was placed in a 50 mL Schlenk tube under a steam of N_2 and stirred overnight at 135 °C. After the reaction mixture was cooled to room temperature, the solvent was removed by vacuum evaporation. The resulting crude product was purified by silica gel column chromatography (petroleum ether, R_f = 0.56) to afford 0.93 g (2.3 mmol) of **3** in 92% yield as white solids: mp 79−80.5 °C; ^{1}H NMR ($CDCl_3$, 300 MHz): δ 2.39 (s, 3H), 7.06 (dd, J = 2.1, 8.1 Hz, 1H), 7.14−7.23 (m, 2H), 7.27 (d, J = 6.9 Hz, 1H), 7.33−7.39 (m, 1H), 7.69 (d, J = 2.1 Hz, 1H), 7.88 (d, J = 8.4 Hz, 1H); ^{13}C NMR ($CDCl_3$, 75 MHz): δ 16.0, 100.0, 125.0, 125.6, 128.7, 129.5, 129.6, 129.7, 133.4, 137.0, 138.4, 139.8, 142.1; HRMS (ESI): 404.8810 ([M + H]$^+$); Calcd for $C_{13}H_{11}BrIS$: 404.8810.

2,2′-Dibromo-2″-methylthio[1,1′:4′,1″]terphenyl (4). To a mixture of **3** (2.02 g, 5.0 mmol), 2-bromophenylboronic acid (1.20 g, 6.0 mmol), K_2CO_3 (2.76 g, 20.0 mmol), PPh_3 (197 mg, 0.75 mmol) and $Pd(OAc)_2$ (56 mg, 0.25 mmol) were added degassed toluene (60 mL) and a 1/1 C_2H_5OH/H_2O (12 mL) degassed mixed solvent under a steam of nitrogen. The reaction mixture was refluxed overnight. The mixture was cooled to room temperature and then extracted with CH_2Cl_2. The combined organic layer was dried over anhydrous Na_2SO_4, filtered, and concentrated under reduced pressure. The resulting mixture was subjected to a silica gel column chromatography (5/1 petroleum ether/CH_2Cl_2, R_f = 0.51) to afford 1.51 g (3.50 mmol) of **4** in 70% yield as white solids: mp 126.5−128.5 °C; ^{1}H NMR ($CDCl_3$, 400 MHz): δ 2.40 (s, 3H), 7.20−7.24 (m, 1H), 7.27−7.41 (m, 7H), 7.43 (dd, J = 1.6, 8.0 Hz, 1H), 7.68 (d, J = 8.0 Hz, 1H), 7.74 (d, J = 1.2 Hz, 1H); ^{13}C NMR ($CDCl_3$, 75 MHz): δ 16.0, 123.1, 123.6, 124.9, 125.5, 127.1, 128.2, 128.5, 129.4, 130.1, 130.5, 131.1, 132.6, 133.2, 137.1, 139.0, 140.9, 141.8, 141.9; HRMS (ESI): 432.9243 ([M + H]$^+$); Calcd for $C_{19}H_{15}Br_2S$: 432.9261.

2,2′-Dibromo-2″-methylsulfinyl[1,1′:4′,1″]terphenyl (5). **4** (117 mg, 0.27 mmol) was first dissolved in a 1:1 mixture of glacial acetic acid and chloroform (8 mL) and then cooled with an ice bath until the solvent was about to freeze. Hydrogen peroxide (30%, 61 mg, 0.54 mmol) was added slowly. The cooling bath was removed, and the mixture was stirred at room temperature for 12 h. Acetic acid was removed by vacuum evaporation, and CH_2Cl_2 was added to the residue. The organic fraction was washed with saturated $NaHCO_3$ solution, dried over Na_2SO_4, filtered, and concentrated under reduced pressure. The resulting mixture was subjected to a silica gel column chromatography (CH_2Cl_2, R_f = 0.24) to afford 113 mg (0.25 mmol) of **5** in 93% yield as white solids: mp 164−165 °C; ^{1}H NMR ($CDCl_3$, 300 MHz): δ 2.47 (s, 3H), 7.27−7.33 (m, 3H), 7.39−7.44 (m, 3H), 7.55 (td, J = 1.2, 7.5 Hz, 1H), 7.64−7.71 (m, 3H), 8.15 (d, J = 7.8 Hz, 1H); ^{13}C NMR ($CDCl_3$, 75 MHz): δ 41.78, 41.84, 123.4, 123.7, 123.9, 124.0, 127.3, 127.9, 128.0, 129.4, 129.7, 130.28, 130.32, 130.9, 131.20, 131.25, 132.7, 132.9, 133.1, 137.5, 139.1, 141.3, 142.0, 144.1; HRMS (ESI): 448.9208 ([M + H]$^+$); Calcd for $C_{19}H_{15}Br_2SO$: 448.9210.

4-Bromo-3-(2-bromophenyl)dibenzothiophene (6). *2-Bromo-3-(2-bromophenyl)dibenzothiophene (7).* Compound **5** (450 mg, 0.10 mmol) was added in portions to stirred concentrated H_2SO_4 (1.35 mL, 3 v/w) in a one-necked, round-bottomed flask at 0−5 °C. The reaction mixture was stirred at room temperature for 2 h. The reaction mixture was poured into ice-cold water (10 mL) and then made basic with aqueous potassium carbonate solution (pH 8). The aqueous layer was extracted with CH_2Cl_2. The combined organic layer was dried over anhydrous Na_2SO_4, filtered, and concentrated under reduced pressure. The resulting mixture was subjected to a silica gel column chromatography (petroleum ether, R_f = 0.61) to afford 373 mg (0.90 mmol) of **6** and **7** in 90% yield as white solids: ^{1}H NMR ($CDCl_3$, 300 MHz): δ 7.27−7.37 (m, 2H), 7.39−7.44 (m, 1H), 7.49−7.52 (m, 2H), 7.69−7.72 (m, 2H), 7.85−7.88 (m, 1H), 8.14−8.17 (m, 1H), 8.44 (s, 1H); ^{13}C NMR ($CDCl_3$, 75 MHz): δ 119.8, 120.0, 121.9, 122.2, 123.0, 123.8, 124.7, 124.8, 125.3, 127.2, 127.5, 129.6, 131.2, 131.3, 132.6, 134.2, 136.8, 138.3, 140.1, 140.3, 141.9; HRMS (MALDI/DHB): 415.8863 (M$^+$); Calcd for $C_{18}H_{10}Br_2S$: 415.8870.

11-(2,4,6-Triisopropylphenyl)-11H-Benzo[b][1]benzoborolo-[2,3-*f*][1]benzothiophene (*anti*-BS-TP). *12-(2,4,6-Triisopropyl-phenyl)-12H-Benzo[b][1]benzoborolo[3,2-g][1]benzothiophene (syn-BS-TP).* To a mixture of **6** and **7** (125 mg, 0.3 mmol) in anhydrous THF (10 mL) was added a hexane solution of *n*-BuLi (0.30 mL, 2.5 M, 0.75 mmol) dropwise by syringe at −78 °C under a steam of nitrogen. The mixture was stirred at the same temperature for 1 h. 2,4,6-Triisopropylphenylboronic acid methyl ester, $TipB(OMe)_2$ (100 mg, 0.20 mL, 0.36 mmol) in anhydrous THF (2 mL) was added to the reaction mixture via syringe. The reaction mixture was warmed to room temperature and stirred overnight. The reaction was quenched with saturated solution of NaCl and the aqueous layer was extracted with CH_2Cl_2. The combined organic layer was dried over anhydrous Na_2SO_4, filtered, and concentrated under reduced pressure. The resulting crude product was purified by silica gel column chromatography (50/1 petroleum ether/ethyl acetate) to afford 59 mg (42%) of ***anti*-BS-TP** (R_f = 0.31) as yellow solids and 28 mg (20%) of mixture of ***syn*-BS-TP** and ***anti*-BS-TP**, which was further purified by preparative TLC to give 18 mg (13%) of ***syn*-BS-TP** (R_f = 0.30) as orange solids. ***anti*-BS-TP**: mp 197−198 °C; ^{1}H NMR ($CDCl_3$, 300 MHz): δ 1.14 (d, J = 6.6 Hz, 12H), 1.34 (d, J = 6.9 Hz, 6H), 2.50 (septet, J = 6.6 Hz, 2H), 2.92 (septet, J = 6.9 Hz, 1H), 7.08 (s, 2H), 7.11 (d, J = 6.9 Hz, 1H), 7.35−7.40 (m, 3H), 7.42 (d, J = 7.2 Hz, 1H), 7.49 (d, J = 7.5 Hz, 1H), 7.77−7.81 (m, 1H), 7.84 (s, 1H), 8.00−8.05 (m, 1H), 8.13 (s, 1H); ^{13}C NMR ($CDCl_3$, 75 MHz): δ 24.1, 24.70, 24.74, 34.3, 35.7, 113.9, 119.8, 120.1, 121.5, 122.8, 124.7, 126.4, 128.2, 128.7, 134.3, 134.9, 135.5, 135.9, 139.2, 146.2, 149.0, 150.2, 151.3, 152.9; HRMS (MALDI/DHB): 471.2419 (M$^+$); Calcd for $C_{33}H_{33}{}^{10}BS$: 471.2427.

***syn*-BS-TP.** mp 194.5−196 °C; ^{1}H NMR ($CDCl_3$, 300 MHz): δ 1.13 (d, J = 6.3 Hz, 12H), 1.36 (d, J = 6.9 Hz, 6H), 2.48 (septet, J = 6.3 Hz, 2H), 2.96 (septet, J = 6.9 Hz, 1H), 7.06−7.09 (m, 3H), 7.31−7.45 (m, 5H), 7.50 (d, J = 7.5 Hz, 1H), 7.64 (d, J = 7.5 Hz, 1H), 8.03 (d, J = 6.6 Hz, 1H), 8.08 (d, J = 8.1 Hz, 1H); ^{13}C NMR ($CDCl_3$, 75 MHz): δ 24.2, 24.4, 25.2, 34.4, 36.3, 116.4, 119.8, 120.2, 121.2, 122.9, 124.3, 126.7, 127.2, 128.7, 134.3, 134.8, 134.9, 136.7, 140.6, 149.45, 149.53, 152.8, 153.1; HRMS (MALDI/DHB): 471.2430 (M$^+$); Calcd for $C_{33}H_{33}{}^{10}BS$: 471.2427.

■ ASSOCIATED CONTENT

Supporting Information

^{1}H spectrum of mixture of **6** and **7**, UV−vis absorption and fluorescence spectra of **BS-TPs** in various solvents, UV−vis absorption and fluorescence spectra of **BS-TPs** and ***anti*-BN-TP** in cyclohexane and the spin-coated films, titration experiments of ***anti*-BS-TP** with F^- and Hg^{2+}, and ^{1}H NMR and ^{13}C NMR spectra of all new compounds. This material is available free of charge via the Internet at http://pubs.acs.org.

■ AUTHOR INFORMATION

Corresponding Author

* E-mail: chzhao@sdu.edu.cn.

Notes

The authors declare no competing financial interest.

■ ACKNOWLEDGMENTS

This work was supported by the National Nature Science Foundation of China (Grants Nos. 21072117, 21272141) and the Promotive Research Fund For Excellent Young and Middle-aged Scientists of Shandong Province (No. BS 2012CL021n).

■ REFERENCES

(1) (a) Watson, M. D.; Fechtenkötter, A.; Müllen, K. *Chem. Rev.* **2001**, *101*, 1267. (b) Li, C.; Liu, M.; Pschirer, N. G.; Baumgarten, M.; Müllen, K. *Chem. Rev.* **2010**, *110*, 6817. (c) Figueira-Duarte, T. M.; Müllen, K. *Chem. Rev.* **2011**, *111*, 7260. (d) Wu, J.; Pisula, W.; Müllen, K. *Chem. Rev.* **2007**, *107*, 718.

(2) (a) Poriel, C.; Rault-Berthelot, J.; Thirion, D.; Barrière, F.; Vignau, L. *Chem.—Eur. J.* **2011**, *17*, 14031. (b) Wu, Y.; Zhang, J.; Bo, Z. *Org. Lett.* **2007**, *9*, 4435. (c) Wu, Y.; Zhang, J.; Fei, Z.; Bo, Z. *J. Am. Chem. Soc.* **2008**, *130*, 7192. (d) Zhou, G.; Baumgarten, M.; Müllen, K. *J. Am. Chem. Soc.* **2007**, *129*, 12211. (e) Jacob, J.; Sax, S.; Piok, T.; List, E. J. W.; Grimsdale, A. C.; Müllen, K. *J. Am. Chem. Soc.* **2004**, *126*, 6987.

(3) (a) Kawaguchi, K.; Nakano, K.; Nozaki, K. *Org. Lett.* **2008**, *10*, 1199. (b) Gu, R.; Hameurlaine, A.; Dehaen, W. *J. Org. Chem.* **2007**, *72*, 7207. (c) Wu, Y.; Li, Y.; Gardner, S.; Ong, B. S. *J. Am. Chem. Soc.* **2005**, *127*, 614. (d) Wakim, S.; Bouchard, J.; Blouin, N.; Michaud, A.; Leclerc, M. *Org. Lett.* **2004**, *6*, 3413.

(4) (a) Kawaguchi, K.; Nakano, K.; Nozaki, K. *J. Org. Chem.* **2007**, *72*, 5119. (b) Kowada, T.; Kuwabara, T.; Ohe, K. *J. Org. Chem.* **2010**, *75*, 906.

(5) (a) Li, H.; Batsanov, A. S.; Moss, K. C.; Vaughan, H. L.; Dias, F. B.; Kamtekar, K. T.; Bryce, M. R.; Monkman, A. P. *Chem. Commun.* **2010**, *46*, 4812. (b) Vehoff, T.; Baumeier, B.; Troisi, A.; Andrienko, D. *J. Am. Chem. Soc.* **2010**, *132*, 11702. (c) Wang, Y.; Parkin, S. R.; Gierschner, J.; Watson, M. D. *Org. Lett.* **2008**, *10*, 3307. (d) Ebata, H.; Miyazaki, E.; Yamamoto, T.; Takimiya, K. *Org. Lett.* **2007**, *9*, 4499.

(6) (a) Yamaguchi, S.; Shirasaka, T.; Akiyama, S.; Tamao, K. *J. Am. Chem. Soc.* **2002**, *124*, 8816. (b) Wakamiya, A.; Mishima, K.; Ekawa, K.; Yamaguchi, S. *Chem. Commun.* **2008**, 579. (c) Levine, D. R.; Siegler, M. A.; Tovar, J. D. *J. Am. Chem. Soc.* **2014**, *136*, 7132.

(7) (a) Ureshino, T.; Yoshida, T.; Kuninobu, Y.; Takai, K. *J. Am. Chem. Soc.* **2010**, *132*, 14324. (b) Furukawa, S.; Kobayashi, J.; Kawashima, T. *J. Am. Chem. Soc.* **2009**, *131*, 14192. (c) Li, L.; Xiang, J.; Xu, C. *Org. Lett.* **2007**, *9*, 4877. (d) Usta, H.; Lu, G.; Facchetti, A.; Marks, T. J. *J. Am. Chem. Soc.* **2006**, *128*, 9034. (e) Chan, K. L.; McKiernan, M. J.; Towns, C. R.; Holmes, A. B. *J. Am. Chem. Soc.* **2005**, *127*, 7662.

(8) (a) Hanifi, D.; Pun, A.; Liu, Y. *Chem.—Asian J.* **2012**, *7*, 2615. (b) Chen, R.-F.; Zhu, R.; Fan, Q.-L.; Huang, W. *Org. Lett.* **2008**, *10*, 2913. (c) Su, H.-C.; Fadhel, O.; Yang, C.-J.; Cho, T.-Y.; Fave, C.; Hissler, M.; Wu, C.-C.; Réau, R. *J. Am. Chem. Soc.* **2006**, *128*, 983. (d) Baumgartner, T. *Acc. Chem. Res.* **2014**, *47*, 1613. (e) Ren, Y.; Baumgartner, T. *J. Am. Chem. Soc.* **2011**, *133*, 1328.

(9) (a) Wade, C. R.; Broomsgrove, A. E. J.; Aldridge, S.; Gabbaï, F. P. *Chem. Rev.* **2010**, *110*, 3958. (b) Jäkle, F. *Coord. Chem. Rev.* **2006**, *250*, 1107. (c) Hudnall, T. W.; Chiu, C.-W.; Gabbaï, F. P. *Acc. Chem. Res.* **2009**, *42*, 388. (d) Hudson, Z. M.; Wang, S. *Acc. Chem. Res.* **2009**, *42*, 1584. (e) Yamaguchi, S.; Wakamiya, A. *Pure Appl. Chem.* **2006**, *78*, 1413. (f) Entwistle, C. D.; Marder, T. B. *Angew. Chem., Int. Ed.* **2002**, *41*, 2927. (g) Chen, P.; Lalancette, R. A.; Jäkle, F. *J. Am. Chem. Soc.* **2011**, *133*, 8802.

(10) (a) Iida, A.; Yamaguchi, S. *J. Am. Chem. Soc.* **2011**, *133*, 6952. (b) Iida, A.; Sekioka, A.; Yamaguchi, S. *Chem. Sci.* **2012**, *3*, 1461. (c) Araneda, J. F.; Neue, B.; Piers, W. E.; Parvez, M. *Angew. Chem., Int. Ed.* **2012**, *51*, 8546. (d) Mercier, L. G.; Piers, W. E.; Harrington, R. W.; Clegg, W. *Organometallics* **2013**, *32*, 6820.

(11) (a) Hatakeyama, T.; Hashimoto, S.; Oba, T.; Nakamura, M. *J. Am. Chem. Soc.* **2012**, *134*, 19600. (b) Wang, X.-Y.; Zhuang, F.-D.; Wang, R.-B.; Wang, X.-C.; Cao, X.-Y.; Wang, J.-Y.; Pei, J. *J. Am. Chem. Soc.* **2014**, *136*, 3764. (c) Wang, X.-Y.; Lin, H.-R.; Lei, T.; Yang, D.-C.; Zhuang, F.-D.; Wang, J.-Y.; Yuan, S.-C.; Pei, J. *Angew. Chem., Int. Ed.* **2013**, *52*, 3117. (d) Agou, T.; Kobayashi, J.; Kawashima, T. *Org. Lett.* **2006**, *8*, 2241. (e) Agou, T.; Kobayashi, J.; Kawashima, T. *Chem.—Eur. J.* **2007**, *13*, 8051.

(12) Chen, D.-M.; Qin, Q.; Sun, Z.-B.; Peng, Q.; Zhao, C.-H. *Chem. Commun.* **2014**, *50*, 782.

(13) Hirose, K.; Miura, S.; Senda, Y.; Tobe, Y. *Chem. Commun.* **2012**, *48*, 6052.

(14) Pandya, V. B.; Jain, M. R.; Chaugule, B. V.; Patel, J. S.; Parmar, B. M.; Joshi, J. K.; Patel, P. R. *Syn. Commun.* **2012**, *42*, 497.

(15) (a) Gao, P.; Beckmann, D.; Tsao, H. N.; Feng, X.; Enkelmann, V.; Pisula, W.; Müllen, K. *Chem. Commun.* **2008**, 1548. (b) Gao, J.; Li, Y.; Wang, Z. *Org. Lett.* **2013**, *15*, 1366. (c) Zhang, S.; Qiao, X.; Chen, Y.; Wang, Y.; Edkins, R. M.; Liu, Z.; Li, H.; Fang, Q. *Org. Lett.* **2014**, *16*, 342.

(16) (a) Dallos, T.; Hamburger, M.; Baumgarten, M. *Org. Lett.* **2011**, *13*, 1936. (b) de Melo, J. S.; Burrows, H. D.; Svensson, M.; Andersson, M. R.; Monkman, A. P. *J. Chem. Phys.* **2003**, *118*, 1550. (c) Wild, A.; Egbe, D. A. M.; Birchner, E.; Cimrová, V.; Baumann, R.; Grummt, U.-W.; Schubert, U. S. *J. Polym. Sci., Part A: Polym. Chem.* **2009**, *47*, 2243. (d) Kobayashi, J.; Kato, K.; Agou, T.; Kawashima, T. *Chem.—Asian J.* **2009**, *4*, 42.

(17) (a) Yamaguchi, S.; Akiyama, S.; Tamao, K. *J. Am. Chem. Soc.* **2001**, *123*, 11372. (b) Kubo, Y.; Yamamoto, M.; Ikeda, M.; Takeuchi, M.; Shinkai, S.; Yamaguchi, S.; Tamao, K. *Angew. Chem., Int. Ed.* **2003**, *42*, 2036.

(18) (a) Solé, S.; Gabbaï, F. P. *Chem. Commun.* **2004**, 1284. (b) Melaimi, M.; Gabbaï, F. P. *J. Am. Chem. Soc.* **2005**, *127*, 9680. (c) Chiu, C.-W.; Gabbaï, F. P. *J. Am. Chem. Soc.* **2006**, *128*, 14248. (d) Lee, M. H.; Agou, T.; Kobayashi, J.; Kawashima, T.; Gabbaï, F. P. *Chem. Commun.* **2007**, 1133. (e) Hudnall, T. W.; Melaïmi, M.; Gabbaï, F. P. *Org. Lett.* **2006**, *8*, 2747.

(19) (a) Sundararaman, A.; Victor, M.; Varughese, R.; Jäkle, F. *J. Am. Chem. Soc.* **2005**, *127*, 13748. (b) Parab, K.; Venkatasubbaiah, K.; Jäkle, F. *J. Am. Chem. Soc.* **2006**, *128*, 12879.

(20) (a) Fu, G.-L.; Pan, H.; Zhao, Y.-H.; Zhao, C.-H. *Org. Biomol. Chem.* **2011**, *9*, 8141. (b) Zhao, Y.-H.; Pan, H.; Fu, G.-L.; Lin, J.-M.; Zhao, C.-H. *Tetrahedron Lett.* **2011**, *52*, 3832. (c) Pan, H.; Fu, G.-L.; Zhao, Y.-H.; Zhao, C.-H. *Org. Lett.* **2011**, *13*, 4830.

(21) (a) Khatua, S.; Schmittel, M. *Org. Lett.* **2013**, *15*, 4422. (b) Zhao, Q.; Liu, S.; Li, F.; Yi, T.; Huang, C. *Dalton Trans.* **2008**, 3836. (c) Zhao, Q.; Cao, T.; Li, F.; Li, X.; Jing, H.; Yi, T.; Huang, C. *Organometallics* **2007**, *26*, 2077.

(22) Gaussian 09, Revision A.02, Frisch, M. J.; Trucks, G. W.; Schlegel, H. B.; Scuseria, G. E.; Robb, M. A.; Cheeseman, J. R.; Scalmani, G.; Barone, V.; Mennucci, B.; Petersson, G. A.; Nakatsuji, H.; Caricato, M.; Li, X.; Hratchian, H. P.; Izmaylov, A. F.; Bloino, J.; Zheng, G.; Sonnenberg, J. L.; Hada, M.; Ehara, M.; Toyota, K.; Fukuda, R.; Hasegawa, J.; Ishida, M.; Nakajima, T.; Honda, Y.; Kitao, O.; Nakai, H.; Vreven, T.; Montgomery, J. A.; Peralta, Jr. J. E.; Ogliaro, F.; Bearpark, M.; Heyd, J. J.; Brothers, E.; Kudin, K. N.; Staroverov, V. N.; Kobayashi, R.; Normand, J.; Raghavachari, K.; Rendell, A.; Burant, J. C.; Iyengar, S. S.; Tomasi, J.; Cossi, M.; Rega, N.; Millam, J. M.; Klene, M.; Knox, J. E.; Cross, J. B.; Bakken, V.; Adamo, C.; Jaramillo, J.; Gomperts, R.; Stratmann, R. E.; Yazyev, O.; Austin, A. J.; Cammi, R.; Pomelli, C.; Ochterski, J. W.; Martin, R. L.; Morokuma, K.; Zakrzewski, V. G. ; Voth, G. A.; Salvador, P.; Dannenberg, J. J.; Dapprich, S.; Daniels, A. D.; Farkas, O.; Foresman, J. B.; Ortiz, J. V.; Cioslowski, J.; Fox, D. J. Gaussian, Inc., Wallingford CT, 2009.

■ NOTE ADDED AFTER ASAP PUBLICATION

This paper was published on the Web on November 4, 2014, with errors in the TOC/Abstract graphic. The corrected version was reposted on November 7, 2014.